RSC Advances

ROYAL SOCIETY OF CHEMISTRY

www.rsc.org/advances

Graphical abstract

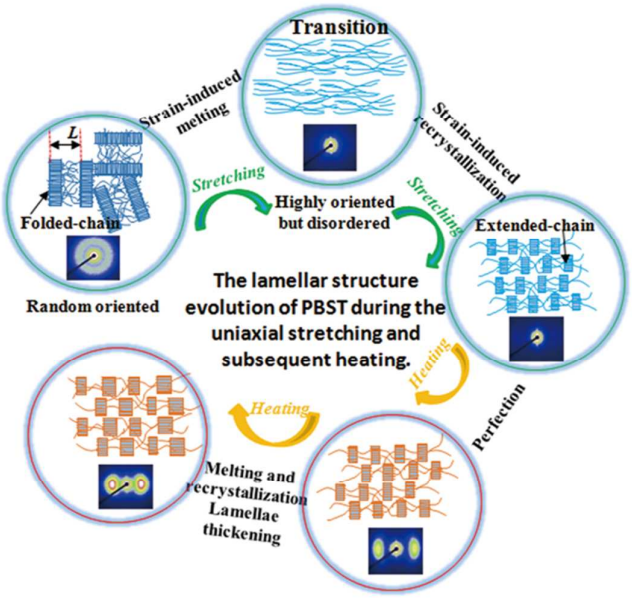

The structural evolution of biodegradable poly(butylene succinate-*co*-terephthalate) copolymer was investigated during the uniaxial stretching and following heating process via in situ small-angle X-ray scattering.

Cite this: DOI: 10.1039/c0xx00000x

www.rsc.org/xxxxxx

ARTICLE TYPE

Lamellae evolution of poly(butylene succinate-*co*-terephthalate) copolymer induced by uniaxial stretching and subsequent heating

Zhenzhen Wei,[a,b] RuiXin Lun, [a,b] Xueqin Lou, [a,b] Feng Tian,[c] Jinyou Lin,*[c] Xiuhong Li,[c] Jianyong Yu[d] and Faxue Li*[a,b]

Received (in XXX, XXX) Xth XXXXXXXXX 20XX, Accepted Xth XXXXXXXXX 20XX
DOI: 10.1039/b000000x

The lamellar structural evolution of biodegradable poly(butylene succinate-*co*-terephthalate) (PBST) random copolymer was investigated under the conditions of uniaxial stretching at 50 °C and then heating from 50 to 150 °C at the strain of 150% with in situ small-angle X-ray scattering (SAXS) technique. A long period referring to the lamellae of processing PBST was calculated, and a schematic for the structural evolution was proposed. It has been found that the lamellar structure experienced remarkable transformation accompanying with the strain-induced melting of lamellae and formation of new lamellae when the strain exceeded 84% at 50 °C during the initial deformation process. After a stretching by 150%, the lamellar structure kept unchanged just with the perfection of lamellae in the following heating process from 50 to 120 °C. Only at relatively high temperature (120 - 150 °C), the long period of lamellae took on a significant increase. Conclusions can be drawn that the lamellar structure of PBST is more sensitive to the strain and only relatively high temperature has prominent impacts on it, which is of great significance to provide targeted design guidance for the manufacturing and application of biodegradable PBST copolymer and also has potential insights into other random and aliphatic-aromatic copolymers.

Introduction

Polymers are subjected substantially to mechanical deformation and thermal treatment during their processing as well as in practical applications, giving rise to the continuous structure changes.[1-3] The mechanical properties of these polymers are determined by their final structures as well as their evolution process.[4-7] Hence, revealing the structural evolution during processing with an aim of controlling the final structure is expected to regulate the mechanical properties of end products and thus extends their applications.

The structure of crystalline polymers, viewed on scale, normally is hierarchical, i.e. from the molecular chains of a few nanometers width to crystalline lamellae of dozens of nanometers thickness and spherulites of several micrometers in diameter.[8, 9] Among them, lamellar structure is one of the most common structural models and possesses alternating crystalline lamella and amorphous region.[10] Actually, the transformation of lamellar structure comes from variation of macromolecular arrangement in the two regions during the processing process, resulting in the whole structural changes. Meanwhile, the presence and change of crystalline and amorphous regions within the polymer enable it to exhibit different levels of rigidity and toughness.[11, 12] Therefore, revealing the lamellar structure developments during dynamic process is essential both in fundamental researches and practical applications.

A wealth of researches have been conducted on the lamellar structure developments during stretching as well as heating using a host of experimental techniques such as small-angle X-ray scattering (SAXS),[12-19] wide-angle X-ray diffraction,[20-26] transmission electron microscopy,[27, 28] Fourier transform infrared microscopy, [29, 30] and atomic force microscopy.[31, 32] Stretching can transform the original spherulite morphology into a highly oriented fibrillar one, where polymeric chains are preferentially aligned along the stretching direction. Based on the results of SAXS experiments, the strain-induced melting and recrystallization were proposed to be responsible for the morphological variation during the deformation.[18, 14, 33]

Meanwhile, a fraction of uniaxial stretching experiments were carried out at different temperatures to explore the influences of temperature on polymeric structure development during stretching.[34-37] The effects of temperature are mainly reflected in the initial crystallinity and chain mobility that vary with the drawing temperature. Just taking the temperature without deformation into consideration, the structural evolution of semi-crystalline polymers has also been extensively investigated during heating and annealing processes.[12, 13, 21, 23, 24, 38, 39] Actually, the molecular mobility mechanism during heating is dependent on crystallization conditions, thermal history and other treatments subjected. Therefore, there has not yet a consistent conclusion for polymers upon heating. Besides, most of the researches mentioned above focused on elucidating the molecular mobility mechanism during the process of stretching and heating

separately. Contrarily, few publications have reported the structural transformation during first stretching and subsequent heating, or heating and then stretching. In fact, the structural changes are of great importance to the polymers that are orderly subjected to the tensile deformation and thermal treatment during their processing process or applications.

Poly(butylene succinate-*co*-terephthalate) (PBST), one kind of biodegradable aliphatic-aromatic copolymer, has spurred much interests in the past decades. We have reported its preparation, structure, properties and application in the form of elastic fibers with high elastic recovery in previous work.[40-42] Recently, the unstable morphologies fundamentally ascribed to the complex structure transformation in the dynamic environments are encountered in the manufacturing of PBST fibers, resulting in relatively poor mechanical properties and low productivity. As a matter of fact, some important semi-crystalline polymers including polypropylene,[34, 43] polyethylene,[37, 44] and poly(ethylene terephalate)[45] have been well documented about their structure developments, which have played positive role in their structure regulation and properties improvement. Thus, it is necessary to elucidate the structure developments of PBST at the lamellar levels during its deformation and/or heating for further practical application in future work. Meanwhile, compared with these important polymers, PBST is a type of random copolymer.[46] Some investigations were carried out on the uniaxial stretching and structural evolution of semi-crystalline block copolymers.[47-49] Therefore, studies on the structural changes of PBST probably have the potential insights into other random copolymers.

In this work, the in situ SAXS technique using synchrotron radiation X-ray in combination with a tensile device and a heating chamber was used to investigate the lamellar structure information during uniaxial stretching and following heating. The sample was initially stretched with a constant strain of 150% under 50 °C and then heated to 150 °C with several isothermal stages under this stable strain. The long period of PBST as well as its evolution was extensively explored, and a schematic for its lamellar structure evolution during the uniaxial stretching and subsequent heating was proposed.

Experimental

Materials and sample preparation

Poly(butylene succinate-*co*-terephthalate) (PBST) copolymer was synthesized by ourselves and the specific reaction conditions and procedures were reported in our previous work.[41] The chemical structure of PBST and its monomers are shown in Scheme 1. The 70 mol% of butylene terephthalate unit was selected by adjusting the feeding ratio of succinic acid to terephthalic acid due to its balance between desirable biodegradability and good mechanical properties.[40,41] The number average molecular weight (M_n) was 50600 g/mol and the polydispersity index was 1.92 through gel permeation chromatography (GPC) measurement. The endothermic peak was located at 180.4 °C in the differential

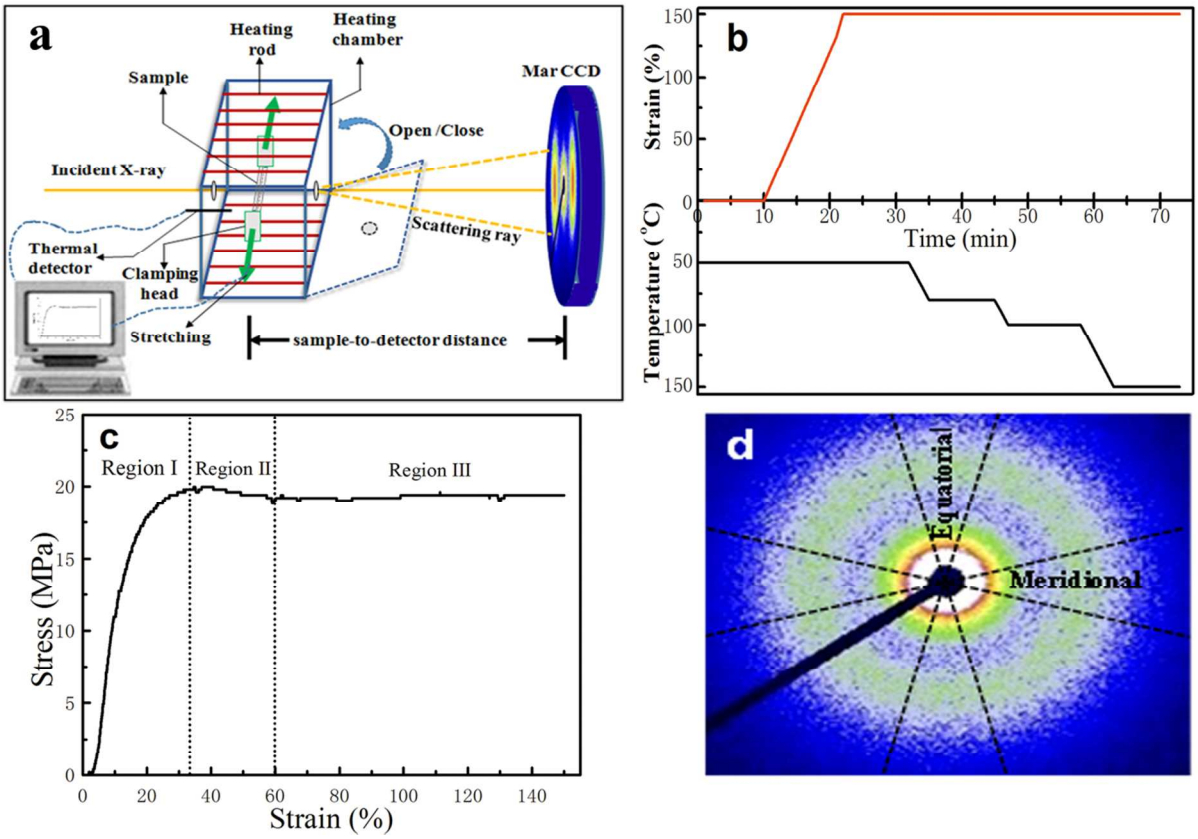

Fig. 1 (a) Schematic representation of the in situ SAXS measurement in this work. (b) A diagram showing the uniaxial stretching and subsequent heating procedures. (c) A typical stress-strain curve of the PBST copolymer. (d) The integration sector of 2D patterns along the meridional (-15-15°) and equatorial (75-105°) direction.

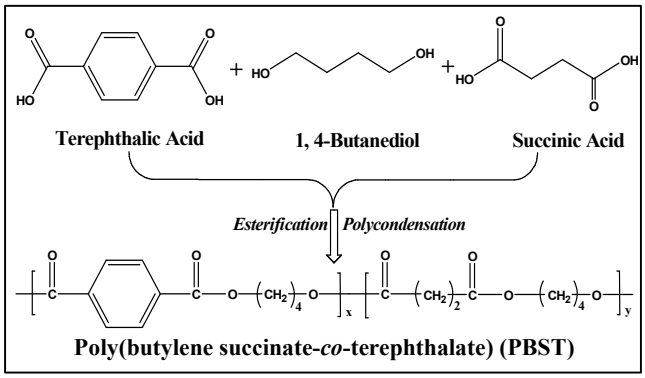

Scheme 1 Illustration showing the chemical structure of as-synthesized PBST.

scanning calorimetry (DSC) measurement and the glass transition temperature was about 13 °C determined by dynamic mechanical analysis (DMA) (shown in supporting information Fig. S1).

The as-prepared PBST was melted at 200 °C in a hot press and kept at this temperature for 5 min. After that, it was naturally cooled down to room temperature. The film was then cut into dumbbell-shaped bar with dimension of 50 mm (length) × 10 mm (neck width) × 0.5 mm (thickness).

In-situ SAXS measurement

SAXS experiments were conducted at the beamline BL16B1 of Shanghai Synchrotron Radiation Facility (SSRF, Shanghai, China). The X-ray wavelength was 0.124 nm and a Mar 165 CCD detector (2048 × 2048 pixels with a pixel size of 82.5 μm) was employed to collect two dimensional (2D) SAXS patterns. The sample-to-detector distance was 2280 mm. The data of blank air were collected to correct the air scattering. A homemade tensile tester with a heating chamber was used for the uniaxial tensile deformation during the in situ experiments. This apparatus can stretch sample symmetrically, beneficial to probe the same position during deformation. The schematic presentation of the device is shown in Fig. 1a.

The detailed experimental procedures are presented in Fig. 1b. The sample with 10 mm in gauge length was first heated to 50 °C and held for 10 min, and then was stretched to a strain of 150% at a constant velocity of 20 μm/s at this temperature. The typical stress-strain curve of PBST copolymer during this process was obtained as shown in Fig. 1c. The stretched sample was further heated to the preset temperatures of 80, 100 and 150 °C at a rate of 10 °C/min under the fixed strain. The real temperature of sample is expected to be ±2 °C than that of chamber. At each temperature stage, the sample was kept for 10 min before heating to higher temperature. The 2D patterns were accumulated over periods of 20 sec during the whole process.

Fit2D software was used to transfer 2D patterns into one dimensional (1D) profiles from the integration sectors demonstrated in Fig. 1d in the form of intensity *vs* q (scattering vector, $q = (4\pi/\lambda)sin(\theta/2)$, where λ is the wavelength of X-ray and θ is the scattering angle). The long period (L, distance between the adjacent lamellae) was calculated from the Bragg equation of $L = 2\pi/q_{max}$, where q_{max} corresponds to the peak position of the 1D SAXS profiles.

Results and discussion

Fig. 1c shows the engineering stress-strain curve of PBST copolymer during uniaxial stretching at 50 °C. The stress first increases to its maximum value at the strain of 32% (i.e., the yield point), and then decreases slightly followed by a stress plateau. The strain-hardening phenomenon was not conspicuous for this sample due to the limited strain to 150% in this case. To elucidate the deformation behaviors of PBST copolymer in detail, the stress-strain curve is divided into three regions, namely region I (0 ≤ strain ≤ 32%), II (32 < strain < 60%) and III (60 ≤ strain ≤ 150).

To investigate the lamellar structure evolution of PBST induced by uniaxial stretching, the 2D SAXS patterns at different applied strains are collected as shown in Fig. 2. After naturally cooled, PBST crystallized into spherulite consisting of many chain-folded lamellae.[40] The SAXS pattern of unstretched sample exhibited a single isotropic scattering ring (strain 0%), indicative of the existence of randomly oriented chain-folded lamellae. [43, 50] With the increasing strain in region I, the patterns gradually became oblate, for that the scattering maximum of SAXS patterns along the meridian shifted to a small angle, whereas that along the equator moved to a large angle. Moreover, the oblate pattern with two big arcs gradually became a two-bar like pattern with the scattering maxima in the meridional direction (strain from 4 to 32%). As the strain increased in region II, the two bars became smeared, short and shifted towards beam center, suggesting that the destruction and fragmentation of lamellar structure prevailed. At the early stage of region III, the two bars remained smearing (strain from 68 to 76%). When the strain reached about 84%, the two-bar like pattern completely disappeared, manifesting that the lamellar structure was possibly breached entirely. Above the strain of 84%, there were no obvious differences in 2D SAXS patterns. Therefore, a general understanding of the structural evolution during deformation was available from the changes of 2D SAXS patterns.

To further explore the evolution involving specific parameters of lamellar structure during the uniaxial stretching, the relation of q *vs*. $I(q)$ in these three regions obtained from the 2D SAXS scattering data through integrating is presented in Fig. 3, from which the long period (L) and the scattering intensity of the peak (I_{max}) are calculated and shown in Fig. 4. In region I (Fig. 3a and c), the changing trends of q_{max} along the meridian and equator are inverse, implying that the interlamellar distances in the two

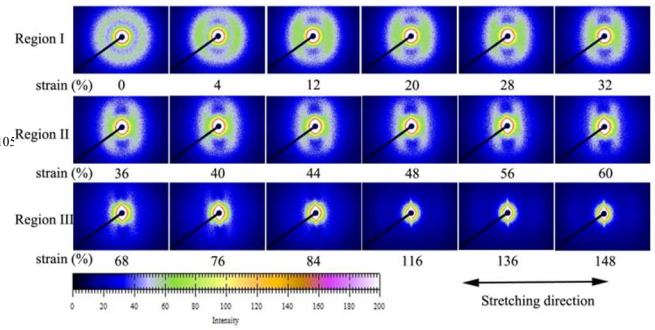

Fig. 2 Selected 2DSAXS patterns at different strains in regions I, II and III.

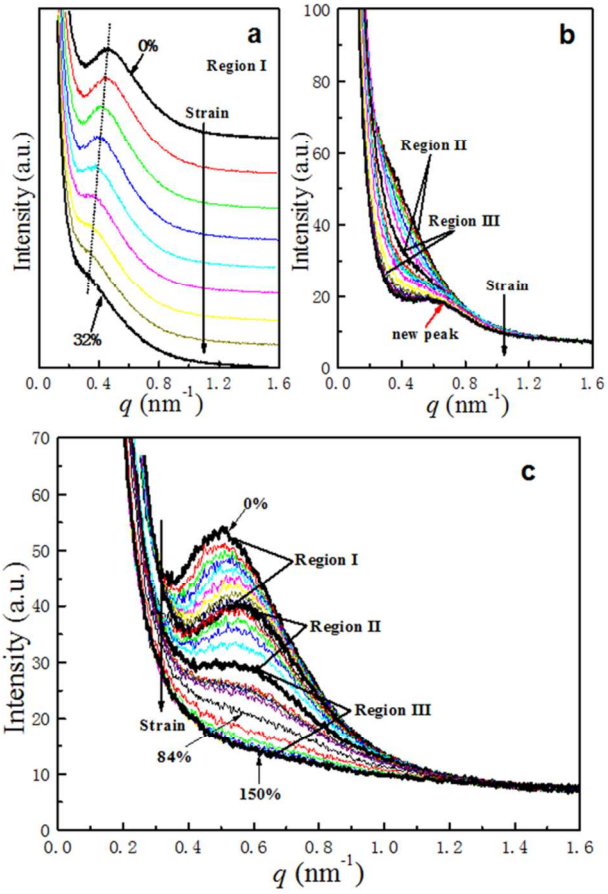

Fig. 3 Selected 1DSAXS profiles during stretching along the (a) and (b) meridional and (c) equatorial direction in regions I, II and III. The profiles of region I in (a) were vertically shifted to clearly show the tendency and avoid overlaps.

directions present opposite development with the increasing strain. Within the strain ranging from 0 to 9%, where the stress increased nearly linearly with the strain, the L value along the meridian increased from 14.2 to 15.5 nm (Fig. 4), up 9.2%, close to the applied strain 9%. This increase is generally attributed to the elastic extension of chains in amorphous region, leading to the macroscopic elastic behavior of the material at a relatively low strain.[18, 34]

As the strain was above 9%, the stress increasing was retarded and the scattering intensity was decreased more distinctly, especially when the yield point was approached. The explanation that a fraction of lamellar structure began to be destroyed after stretched by 9% was found to be reasonable for such stress response in this case, combing the following phenomenon in Fig. 4, the I_{max} at 32% strain decreased quite substantially from that of the original sample. The thickness change of the sample should not be taken into consideration for the decreased intensity during the very small deformation, while the strain-induced melting should be the reason for the prominent decrease. The result agreed very well with previous report by Hsiao et al.[14] Besides, the long period along the equator displayed in Fig. 4 gradually decreased with the strain, as expected from the deformation along the meridional uniaxial stretching.

In the yielding region (region II), the behavior of strain-induced melting became more evident. As shown in Fig. 3b, the intensity distribution curves changed to monotonic waning with the strain in this region, and it was uneasy to point out the values of q_{max}, implying that periodical structure became increasingly unclear due to the melting of original lamellar structure. Most of molecular chains escaped from the original chain-folded lamellae into the amorphous region, causing little electron density difference and thus an inconspicuous periodical structure. The value of long period got indistinct but had a tendency to increase due to the destruction of some lamellae, resulting in the enlargement of average distance between the remaining lamellae.

Fig. 3c shows that the 1D SAXS profiles integrated from equatorial direction at different strains in region II. The peak moved to a high q value, suggesting that some lamellae aligned perpendicularly to the stretching direction were still preserved, and its long period decreased with the rising strain. This decrease could be attributed to the insertion of fragmental lamellae and/or reorientation of lamellae to the stretching direction.[18] Furthermore, the above results demonstrated that the strain-induced melting process was directionally dependent. Therefore, the lamellae along the stretching direction were melted first and faster than that of the lamellae aligned perpendicularly to the stretching direction.

It had to point out that the four-point patterns occurred in many other semi-crystalline polymers under deformation in the yielding region[14, 17, 18, 35] were not observed here. The presence of four-point patterns suggested the fragmentation of lamellae and those fragmented lamellae were tilted against the stretching direction and/or had a checkerboard arrangement to minimize the stress concentration at the lamellae.[12, 14, 18] No four-point patterns observed here could be explained as: firstly, the relatively weak scattering intensity of tilted lamellae was covered by the two bars; secondly, there still were lamellae aligned perpendicularly to the stretching direction, and it was unnecessary for other fragmented lamellae to tilt against the stress concentration. As a result, the slightly negative slope in the yielding region was reasonable due to the presence of lamellae aligned perpendicularly to the stretching direction.

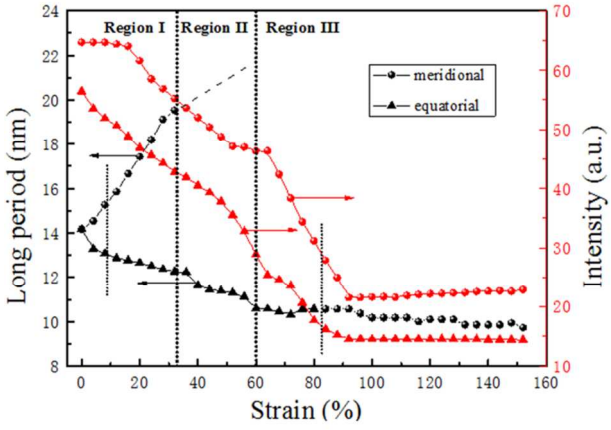

Fig. 4 The long period and scattering intensity of the peak as a function of strain calculated from Fig. 3.

In region III, above the strain of 84%, there were no obvious differences in 2D SAXS patterns possibly due to the very weak intensity, but a new peak corresponding to higher q value compared with the initial peak appeared in the 1D SAXS profiles (Fig. 3b), indicating that a new lamellar structure possibly with extended-chains was formed with further deformation (i.e. strain-induced crystallization) and aligned along the stretching direction. The intensity of this peak slightly augmented as the strain increased, while its position stayed nearly fixed. Some researchers found the smaller long period in the newly formed crystals (i.e. thinner lamellae) than the original lamellae was attributed to the lower stretching temperature than the crystallization temperature of original sample.[17, 51] This is consistent with our observation, since the stretching temperature was 50 °C while the crystallization temperature of PBST sample was about 140 °C (seen in Fig. S1).

Within the strain range of 60 - 84%, the scattering intensity along equator (Fig.3c) gradually transferred to monotonic decrease, similar to the intensity variation along the meridian of region II (Fig. 3b), indicating that the amount of the lamellae perpendicularly to the stretching direction was declining due to their melting and orientation to the stretching direction.[18, 34] When the strain reached about 84%, these lamellae were completely melted and oriented along the stretching direction, with a result of almost unchanged 1D profiles in the equator in further stretching. If the newly oriented lamellae did not melt before the strain of 84%, there should be two peaks including the oriented and newly formed lamellae which appeared with the increasing strain. There was no coincidence that the two kinds of lamellae were identical in the interlamellar distance because the orientation along the stretching direction would not bring about such a large change in long period (declined from 19.4 to 10.5 nm).[52] However, there was only one peak occurred in the meridian and remained constant as the strain was above 84%, indicating that the newly oriented lamellae also were entirely melted before the strain of 84%. In other words, strain-induced melting for those lamellae aligned not along stretching direction was accompanied with their orientation process. At the strain of about 84%, a transitional structure (disordered but with highly oriented molecular chains) was formed. After that, the newly oriented chains together with the original chains along the stretching direction crystallized during the further deformation, leading to the formation of new lamellae.

The scattering intensity gradually lessened along both the meridian and equator as the strain went up with an exception of the range where new lamellae were formed (Fig. 4). The decreased and quite weak intensity at the beginning of deformation could result from the small electron density difference between crystal phases and amorphous phases during melting, the reorientation of lamellae, while the reduced thickness of the sample at large deformation should be primarily responsible for this.[43] It should be noted that the 2D SAXS patterns showed no scattering streak in the equatorial direction near the beam stop when the applied strain was above yield point (strain from 48 to 84% in Fig. 2). It could be an explanation that no micro-voids was formed during the stretching period possibly due to the slow deformation rate and good ductility of PBST.[35, 43] However, with the increasing strain, especially at the later stage

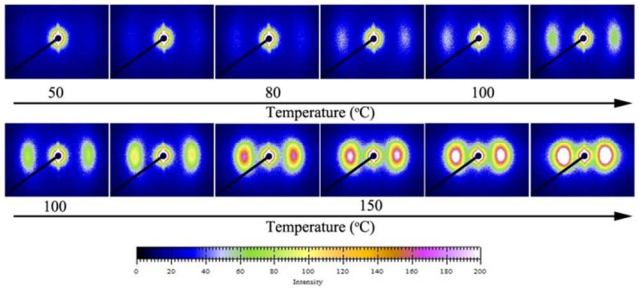

Fig. 5 Selected 2D SAXS patterns of PBST during heating under 150% strain.

of deformation, another relatively weak scattering streak in the equatorial direction appeared and looked stronger with the elevating strain. Judging by its weak and changing intensity, the streak was probably fairly contributed to the formation of fibrillar structure.

To understand the effects of heating on the lamellar structure of PBST copolymer under relatively small strain, after thermally annealed at 50 °C under the strain of 150%, PBST was further heated to 150 °C intermittently as shown in Fig. 1b, and some corresponding 2D SAXS patterns are presented in Fig. 5. The two-bar like patterns along the meridian gradually became noticeable, showing the lamellar structure again prevailed during the heating process. When the temperature approached 100 °C, the two bars changed into two lobes, whose contours were enlarged with the increasing temperature. The streak in the equator was nearly unchanged in the process of heating. The general representation of the two-bar like pattern means that the lamellae are more regularly spaced and of equal thickness, while the two-lobe like pattern signifies the nonuniform thickness and distance between the lamellae.[44] So from the transformation of these patterns, a general understanding about the lamellae changes during heating can be acquired.

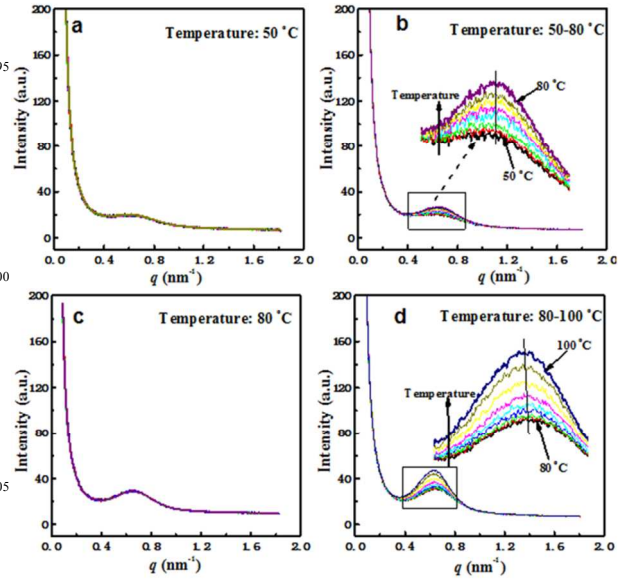

Fig. 6 Selected 1D SAXS profiles along the meridian at the temperature range of 50 - 100 °C.

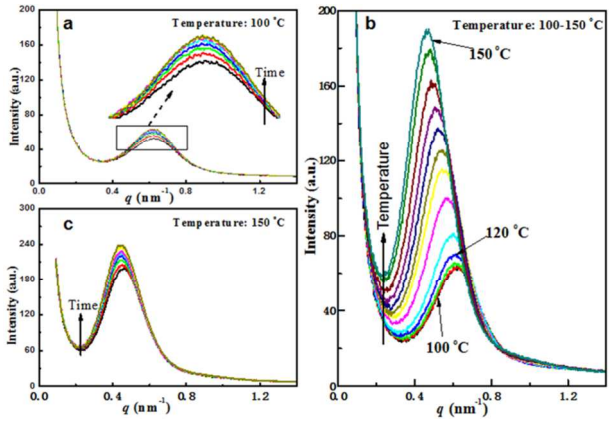

Fig. 7 Selected 1D SAXS profiles along the meridian at the temperature range of 100 - 150 °C.

The detailed effects of temperature on the development of lamellar structure of stretched PBST (strain 150%) can be grasped according to Fig. 6 and 7, which present the selected 1D SAXS profiles at the temperatures from 50 to 100 °C and 100 to 150 °C, respectively. For simplicity, we divided the temperature range into two sections: relatively low temperature region (50 – 100 °C) and high temperature region (100 - 150 °C). When the sample was under strain during heating, stress relaxation of molecular chains should be taken into consideration. Fig. S2 displays the stress relaxation curve of PBST under the strain of 150% as a function of time. As expected, the stress decreased sharply at the relatively low temperature with the increasing time and gradually reached a roughly constant value after about 30 min. Consequently, the influence of stress relaxation of molecular chains should not be ignored in the relatively low temperature region, whereas that in the second region is supposed to be overlooked.

In the low temperature region as shown in Fig. 6, as the sample was thermally annealed at 50 °C, the new peak formed at the late stage of deformation still existed and no further changes in its position and intensity were detected with the annealing time (just shown as the overlapped profiles in Fig. 6a). The similar feature also can be observed during the isothermal period of 80 °C in Fig. 6c. These findings indicated that no changes in lamellar structure came up when the sample was held at relatively low temperature. In comparison with Fig. 7a and c, in the isothermal periods of 100 and 150 °C, the q_{max} remained unchanged but the scattering intensity increased, suggesting that higher temperature was more conducive to perfect the lamellae than the relatively low temperature at the same isothermal time. It is possible that the increase of scattering intensity can be realized if we prolong the annealing time at the low temperature according to the well-known time-temperature equivalence principle.

During the heating of 50 - 80 °C and 80 - 100 °C process displayed in Fig. 6b and d, respectively, the scattering intensity ramped up with the almost invariable q_{max}. The rising in scattering intensity was resulted from the increase of electron density difference, which probably was due to the different thermal expansion of crystal and amorphous regions of lamellae, perfection of lamellae, and melting of small crystals during the heating process.[38] On the other hand, the constant long period (corresponding to the invariable q_{max}) can be ascribed to the balance between the relaxation of stretched amorphous chains inducing long period decrease, and the melting of small lamellae and increasingly chain mobility causing long period increase in the thickness of amorphous region.

In the high temperature region (Fig. 7b), the q_{max} value was initially unchanged with the increasing scattering intensity. Nevertheless, as the temperature went up to 120 °C, the q_{max} continuously shifted to the left side and the scattering intensity also exhibited a prominent rising. In this period, the increased long period can be attributed to the two main reasons as followed: firstly, the melting of small and thinner lamellae due to the high molecular mobility leads to the thickness increase in amorphous region; secondly, the recrystallization of partial melted crystals causes the thickening of crystalline region in the lamellar structure.[38]

The changes occurred in this period were so significant that it was necessary to find out which one of the two factors or whether both of them on earth played the dominant role in enlarging the long period. It can be verified by exploring the specific thickness variations of the crystal and amorphous region in this process, assuming the two-phase model of lamellar nanostructure. The one-dimensional correlation function $\gamma(r)$ in the following equation can be applied to estimate the morphological variables.

$$\gamma(r) = \frac{\int_0^\infty I(q)\cos(qr)dq}{\int_0^\infty I(q)dq}$$

where r is the location measured along a trajectory normal to the lamellar surfaces. The resultant correlation function curves are presented in Fig. 8a. Inset of Fig. 8a shows how the long period(L) and crystalline thickness (l_c) are determined. Generally, it is not a possible to decide whether it is the amorphous or the crystalline thickness that is read out from the correlation function without prior knowledge of the crystallinity.[12] However, the crystallinity of the sample used in the present study was 30 - 40% according to the results of WAXD measurement (seen in Fig. S3), ensuring the assignment of smaller value obtained from correlation function to the thickness of crystalline region (l_c). The amorphous thickness (l_a) can be obtained by subtracting the crystalline thickness from the long period ($l_a = L - l_c$).

The calculated values of L, l_c and l_a as a function of temperature are given in Fig. 8b. At the beginning of the heating, all values were nearly unchanged possibly because the molecular chains were in a metastable state after the thermal treatment in the foregoing low temperature region. However, the L, l_c and l_a increased simultaneously at higher temperatures (over 120 °C). The increase of l_a should be attributed to the melting of small and thinner lamellae, while the enlargement of l_c was mainly due to the recrystallization of partial melted crystals during the heating process, together leading to the increasing long period. Moreover, it could be founded that the recrystallization of molecular chains still exists at high temperature (about 20 - 30 °C lower than the melting temperature of PBST) where the chain mobility was very high. The lamellae thickening at different temperatures were asynchronous and thus irregular crystals were formed, corresponding to the results shown in the 2D SAXS patterns.

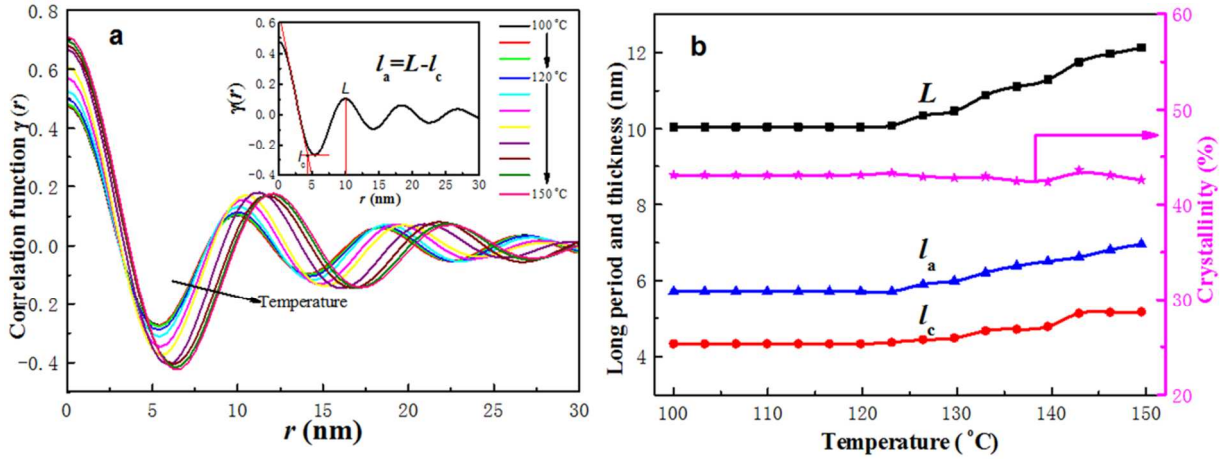

Fig. 8 (a) Correlation function calculated from the 1D SAXS profiles in Fig. 7b. (b) Values of long period L, crystal thickness l_c, amorphous thickness la and inner crystallinity (l_c/L) calculated from the correlation functions using a two-phase model. The inset of (a) demonstrates how the values are determined.

The inner crystallinity of the lamellae as defined by the ratio of the crystal thickness to the long period is also presented in Fig. 8b. The inner crystallinity obtained by SAXS represents the volume fraction of crystallites within the lamellae stacks.[16] It was distinctly seen that the inner crystallinity roughly kept unchangeable with the rising temperature despite a little fluctuation, indicative of the constant volume fraction of crystallites within the lamellar structure and independence on the morphology of the lamellae. The constant inner crystallinity was mainly attributed to the coexistence of melting and recrystallization of crystals in lamellae, which was in accordance with the thickness increase of crystalline and amorphous regions. The formation of perfect lamellae occurred during the melting and recrystallization could be the explanation to the increased scattering intensity.

Fig. 9 presents a schematic illustration of lamellar structural evolution of PBST random copolymer during in situ stretching and heating on the basis of SAXS examination. Within the strain ranging from 0 to 9%, where the stress increases nearly linearly with the strain, the increase of long period is mainly due to the elastic elongation of molecular chains in amorphous region. After the strain of above 9%, the strain-induced melting occurs to cause a nonlinear change of stress-strain curve. The melting behavior of lamellae becomes dominant in the yielding region (32 - 60%), where the stress-stain curve displays a slightly negative slope. When the strain reaches 84%, the lamellar structure transfers into a disordered structure with highly oriented chains, indicating the strain-induced melting is terminated and no lamellae exist. Meanwhile, before the strain of 84%, the unoriented lamellae gradually aligned along the stretching direction accompanying with their destruction. As the strain further increases (above 84%), new and thinner lamellae with extended chains are formed and the population of the strain-induced crystals rises. During the heating period of 50 to 120 °C, the long period changes little while the scattering intensity increases, meaning that the lamellar thickness is nearly unchanged but lamellae are perfected at this relatively low heating temperatures. However, when the temperature is above 120 °C, the lamellar structure is significantly altered with the increasing thickness of both crystal and amorphous phases, which should be attributed to the lamellae thickening caused by the melting, recrystallization and high chain mobility in this high temperature region.

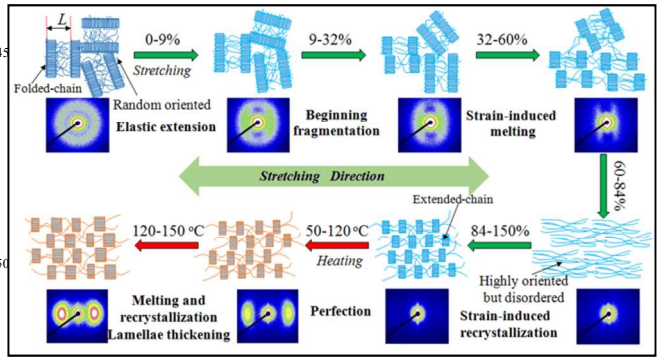

Fig. 9 A schematic representing the lamellae evolution of PBST copolymer during the uniaxial stretching and subsequent heating.

Different from other polymers reported, the lamellar structure changes of PBST random copolymer under uniaxial stretching exhibit a transitional state without lamellae despite experiencing the similar strain-induced melting and recrystallization. The evolution of lamellar structure of PBST random copolymer should be mainly attributed to the synchronous changes of amorphous and crystalline regions. The lamellar structural evolution of PBST copolymer could provide possible enlightenment for the structure changes of other random copolymers, especially those with complicated chain arrangement and the uncertainty of crystalline units.

Conclusions

In summary, we have presented the lamellae evolution of PBST during the uniaxial stretching and subsequent heating by using in situ SAXS with a thermo-mechanical coupled equipment. In the initial deformation process, the lamellar structure experienced remarkable transformation, accompanying with the strain-induced

melting of lamellae and the formation of new lamellae above the strain of about 84% at 50 °C. During the following heating process, the lamellar structure kept unchanged when heated from 50 to 120 °C. Only at relatively high temperature (120 - 150 °C), did the long period of lamellae significantly increase with the thickness enlargement of both amorphous and crystal phases, which was attributed to the melting and recrystallization at high temperature. Hence, it is concluded that the lamellar structure of PBST is more sensitive to the strain and only relatively high temperature has prominent impacts on it, which is vital to design the manufacturing and application of PBST copolymer and sheds lights on the investigation of other random copolymers.

Acknowledgments

This work has been financially supported by National Natural Science Foundation of China (Nos. 51303200 and 11305249), the Chinese Universities Scientific Fund (14D310116), Shanghai Natural Science Fund (14ZR1400300), and National Basic Research Program of China (Nos. 2011CB606104 and 2011CB605604). Additionally, the beamline BL08U1A of SSRF is appreciated.

Notes and references

[a] *Key Laboratory of Textile Science &Technology, Ministry of Education, China;*
[b] *College of Textiles, Donghua University, Shanghai201620, China;Fax: +86-21-67792627; Tel:+86-21-67792803; E-mail: fxlee@dhu.edu.cn*
[c] *Shanghai Synchrotron Radiation Facility, Shanghai Institute of Applied Physics, Chinese Academy of Sciences, Shanghai 201204, China. E-mail: Jinyoulin82@gmail.com*
[d] *Modern Textile Institute, Donghua University, Shanghai 200051, China*

† Electronic Supplementary Information (ESI) available: [Thermal analysis curves of PBST copolymer (Fig. S1). The stress relaxation curve of PBST copolymer during the heating process as a function of time (Fig. S2). Peak fitting of XRD curve of PBST copolymer using the software of JADE 5.0 and its corresponding result of crystallinity calculated using the equation X_c= area of crystals peak / total area (Fig. S3).]. See DOI: 10.1039/b000000x/

1 A. Peterlin, *Colloid and polymer science*, 1987, **265**, 357-382.
2 D. Wang, C. Shao, B. Zhao, L. Bai, X. Wang, T. Yan, J. Li, G. Pan and L. Li, *Macromolecules*, 2010, **43**, 2406-2412.
3 K. Cui, L. Meng, N. Tian, W. Zhou, Y. Liu, Z. Wang, J. He and L. Li, *Macromolecules*, 2012, **45**, 5477-5486.
4 M. Failla and L. Mandelkern, *Macromolecules*, 1993, **26**, 7167-7175.
5 M. Kennedy, A. Peacock and L. Mandelkern, *Macromolecules*, 1994, **27**, 5297-5310.
6 Z. Bartczak, *Macromolecules*, 2005, **38**, 7702-7713.
7 N. Tian, W. Zhou, K. Cui, Y. Liu, Y. Fang, X. Wang, L. Liu and L. Li, *Macromolecules*, 2011, **44**, 7704-7712.
8 J. Ruokolainen, G. t. Brinke and O. Ikkala, *Advanced Materials*, 1999, **11**, 777-780.
9 P. H. Nam, P. Maiti, M. Okamoto, T. Kotaka, N. Hasegawa and A. Usuki, *Polymer*, 2001, **42**, 9633-9640.
10 G. R. Strobl and G. R. Strobl, *The physics of polymers*, Springer, 1997.
11 Y. Men, J. Rieger and G. Strobl, *Phys. Rev. Lett.*, 2003, **91**, 095502.
12 Z. Jiang, Y. Tang, J. Rieger, H. F. Enderle, D. Lilge, S. V. Roth, R. Gehrke, Z. Wu, Z. Li and X. Li, *Eur.Polym. J.*, 2010, **46**, 1866-1877.
13 A. M. Jonas, T. Russell and D. Yoon, *Colloid Polym. Sci.*, 1994, **272**, 1344-1351.
14 L. Z. Liu, B. S. Hsiao, B. X. Fu, S. Ran, S. Toki, B. Chu, A. H. Tsou and P. K. Agarwal, *Macromolecules*, 2003, **36**, 1920-1929.
15 T. Miyazaki, A. Hoshiko, M. Akasaka, T. Shintani and S. Sakurai, *Macromolecules*, 2006, **39**, 2921-2929.
16 Y. Tang, Z. Jiang, Y. Men, L. An, H. F. Enderle, D. Lilge, S. V. Roth, R. Gehrke and J. Rieger, *Polymer*, 2007, **48**, 5125-5132.
17 Z. Jiang, Y. Tang, J. Rieger, H.-F. Enderle, D. Lilge, S. V. Roth, R. Gehrke, W. Heckmann and Y. Men, *Macromolecules*, 2010, **43**, 4727-4732.
18 T. Kamal, T. J. Shin and S. Y. Park, *Macromolecules*, 2012, **45**, 8752-8759.
19 L. Li and W. H. de Jeu, *Macromolecules*, 2004, **37**, 5646-5652.
20 S. Ran, X. Zong, D. Fang, B. S. Hsiao, B. Chu and R. A. Phillips, *Macromolecules*, 2001, **34**, 2569-2578.
21 T. Konishi, K. Nishida and T. Kanaya, *Macromolecules*, 2006, **39**, 8035-8040.
22 D. Kawakami, C. Burger, S. Ran, C. Avila-Orta, I. Sics, B. Chu, S.-M. Chiao, B. S. Hsiao and T. Kikutani, *Macromolecules*, 2008, **41**, 2859-2867.
23 A. Sanz, A. Nogales, T. A. Ezquerra, M. Soccio, A. Munari and N. Lotti, *Macromolecules*, 2009, **43**, 671-679.
24 J. Zhao, Z. Wang, Y. Niu, B. S. Hsiao and S. Piccarolo, *J. Phys. Chem. B*, 2011, **116**, 147-153.
25 J. Cai, B. S. Hsiao and R. A. Gross, *Macromolecules*, 2011, **44**, 3874-3883.
26 H. R. Yang, J. Lei, L. Li, Q. Fu and Z. M. Li, *Macromolecules*, 2012, **45**, 6600-6610.
27 J. Li, W. Cheung and C. Chan, *Polymer*, 1999, **40**, 3641-3656.
28 J. Li, W. Cheung and C. Chan, *Polymer*, 1999, **40**, 2089-2102.
29 G. Lamberti, V. La Carrubba, S. Piccarolo and V. Brucato, *Polym. Bull.*, 2003, **50**, 413-420.
30 G. Lamberti, G. W. Peters and B. A. Schrauwen, *Polym. Bull.* 2003, **50**, 405-411.
31 V. Ferreiro and G. Coulon, *J. Polym. Sci. Pt. B-Polym. Phys.*, 2004, **42**, 687-701.
32 Y. Koike and M. Cakmak, *Macromolecules*, 2004, **37**, 2171-2181.
33 S. Ran, X. Zong, D. Fang, B. S. Hsiao, B. Chu, P. Cunniff and R. Phillips, *J. Mater. Sci.*, 2001, **36**, 3071-3077.
34 Z. Cai, Y. Zhang, J. Li, F. Xue, Y. Shang, X. He, J. Feng, Z. Wu and S. Jiang, *Polymer*, 2012, **53**, 1593-1601.
35 Y. Mao, X. Li, C. Burger, B. S. Hsiao and A. H. Tsou, *Polymer*, 2013, **54**, 1432-1439.
36 B. Xiong, O. Lame, J. Chenal, C. Rochas, R. Seguela and G. Vigier, *Polymer*, 2013, **54**, 5408-5418.
37 B. Xiong, O. Lame, J.-M. Chenal, C. Rochas, R. Seguela and G. Vigier, *Polymer*, 2014, **55**, 1223-1227.
38 K. Krüger and H. Zachmann, *Macromolecules*, 1993, **26**, 5202-5208.
39 Y. Mao, F. Zuo, J. K. Keum, B. S. Hsiao, D. W. Thurman and A. H. Tsou, *J. Polym. Sci. Pt. B-Polym. Phys.* 2010, **48**, 26-32.
40 F. X. Li, S. L. Luo, J Zhang and J. Y. Yu, *J Therm Anal Calorim.,* 2013, **113**, 915-21.
41 S. L. Luo, F. X. Li, J. Y. Yu and A. Cao, *J. Appl. Polym. Sci.*, 2010, **115**, 2203-2211.
42 F. X. Li, S. L. Luo, J. Zhang and J. Y. Yu, *J. Therm. Anal. Calorim.*, 2013, **113**, 915-921.
43 F. Zuo, J. K. Keum, X. Chen, B. S. Hsiao, H. Chen, S. Y. Lai, R. Wevers and J. Li, *Polymer*, 2007, **48**, 6867-6880.
44 E. Heeley, T. Gough, D. Hughes, W. Bras, J. Rieger and A. Ryan, *Polymer*, 2013, **54**, 6580-6588.
45 Z. G. Wang, Z. Y. Xia, Z. Q. Yu, E. Q. Chen, H. J. Sue, C. C. Han and B. S. Hsiao, *Macromolecules*, 2006, **39**, 2930-2939.
46 F. Li, X. Xu, Q. Hao, Q. Li, J. Yu and A. Cao, *J. Polym. Sci. Pt. B-Polym. Phys.,* 2006, **44**, 1635-1644.
47 I. Pereira and R. Oréfice, J. Mater. Sci., 2010, 45, 511-522.
48 I. Pereira and R. Oréfice, Macromol.Symp., 2011, 299/300, 190-198.
49 M. Bothe and T. Pretsch, J. Mater. Chem. A., 2013, 1, 14491-14497.
50 A. Nogales, I. Sics, T. A. Ezquerra, Z. Denchev, F. J. Balta Calleja and B. S. Hsiao, Macromolecules, 2003, 36, 4827-4832.
51 A. Peterlin and F. Balta-Calleja, Kolloid-Zeitschrift und Zeitschrift für Polymere, 1970, 242, 1093-1102.
52 A. Peterlin, J. Mater. Sci., 1971, 6, 490-508.